Vinylpyrimidine-Functionalized Triphenylamines: Bimodal Molecular Switches and Multilevel Systems

Olivier Alévêque, Sylvain Achelle, Lionel Sanguinet

ChemPhotoChem

Research Articles
doi.org/10.1002/cptc.202200201

Chemistry Europe
European Chemical Societies Publishing

www.chemphotochem.org

Vinylpyrimidine-Functionalized Triphenylamines: Bimodal Molecular Switches and Multilevel Systems

Olivier Alévêque,[a] Sylvain Achelle,*[b] and Lionel Sanguinet*[a]

Due to their numerous potential applications, the interest for the elaboration of new molecular switch has never stop to grow. Among them, multi-modal systems, where the switching between two different metastable states can be induced by using indifferently several kinds of stimulation, have a special place. In this study, we present our efforts to develop a class of multi-modal systems based on the association of a triphenylamine core with vinylpyrimidine units that exhibits nice acido and electrochromic properties. The most performant ones can present up to three different forms allowing to modulate their absorption and luminescence properties over three discrete levels. In order to provide limitations and outlooks for such systems, their switching behaviors have been rationalized by the help of DFT and TD-DFT calculations.

Introduction

Driven by their numerous application fields, the interest in the elaboration of multi-addressable materials has never stop to grow in the last two decades. Presenting the possibility to switch reversibly between two different states,[1] these systems allow the modulation of a molecular physicochemical property such as color, luminescence or conductivity, to name a few, by application of an external stimulation.[2] To design a molecular system able to respond to at least two different kinds of stimulation, generally referenced as multi-responsive molecular system, several strategies can be followed as attested by the numberless of sequential and orthogonal photo-responsive systems,[3] molecular logic systems[4] and molecular machines[5] reported so far. In such purpose, the combination of two different kind of switchable units in molecular or supramolecular assembly[6] conducts logically to multi-responsive systems. At the opposite to such complex assemblies, this combination can be simply resumed to the introduction of simple functional groups on common switchable unit. As example the introduction of amine group[7] or azoheterocycle[8] known for their acid-base responses on an azobenzene moiety as photochromic unit conducts to pH and photo-sensitive systems. Another strategy is based on the insertion of some switchable units exhibiting an intrinsic multi-state character such as spiropyrans,[9] diarylethene,[10] or Stenhouse adduct[11] to name a few. However, changing the nature of the stimulation (pH change, electrochemical potential, light irradiation) leads in these systems to the generation of different states exhibiting diverse physico-chemical properties and complex switching behavior.

Beside them, some multi-modal molecular switches have been also reported. In these particular systems, the conversion between both states can be achieved by using indifferently two different kinds of stimuli. As example, some of us have particularly studied benzazo-oxazolidine derivatives,[12] where a pH change, an electrochemical potential and a light irradiation can be used indifferently to switch between their colorless and colorful forms.

In our quest to develop other multi-modal molecular systems exhibiting halo- and electrochromic properties, triarylamine units have particularly drawn our attention. In fact, the triphenylamine fragment constitutes the basic node of an important group of modern electroactive functional materials[13] especially for organic dye-sensitized and perovskite solar cells applications.[14] Numerous studies have reported their chemical functionalization in order to introduce different substituents on the phenyl ring or to expand the π-conjugated system to tune their molecular properties in particular their electrochemical behavior.[15] Introducing some (hetero)aromatic or donor substituents on the different *para* position of the triphenylamine unit leads generally to a decrease of the oxidation potential.[15–16] More importantly, the corresponding radical cation generated under oxidation is largely stabilized. Indeed, this later is known to undergo a spontaneous dimerization process leading to tetraphenylbenzidine.[17] when no substituent is present in *para* positions.

Generally used as an efficient electron donating group, the triarylamine moieties have been combined with many other addressable units such as some redox active complexes[18] or photoactive units.[19] In such context, their combination with some azaheterocycles acting as pH sensitive unit has already lead to interesting molecular systems allowing a modulation of their color, nonlinear optical (NLO) and/or luminescence properties by pH changes. Indeed, contrary to the triphenyl-

[a] Dr. O. Alévêque, Dr. L. Sanguinet
Univ Angers, CNRS, MOLTECH-ANJOU, SFR MATRIX 49000 Angers (France)
E-mail: lionel.sanguinet@univ-angers.fr
[b] Dr. S. Achelle
Univ Rennes, CNRS
Institut des Sciences Chimiques de Rennes – UMR 6226
35000 Rennes (France)
E-mail: sylvain.achelle@univ-rennes1.fr

Supporting information for this article is available on the WWW under https://doi.org/10.1002/cptc.202200201

amine unit, azaheterocycles such as pyridine or diazines can be easily protonated leading to corresponding azolium unit acting as strong electron withdrawing group.[20] With a triphenylamine unit acting as a strong electron donor, the protonation of the azaheterocycle promotes the redistribution of the charge density (due to an important internal charge transfer) leading to a strong bathochromic effect on the maximum absorption wavelength.[20] When blue-emitting azaheterocyclic chromophores are used, this protonation has a drastic impact of their luminescence properties which conducts to generate orange-emissive acidified species or non-emissive materials.[21] Some of us have demonstrated that white light emitting material, potentially useful for OLED applications, can be generated by a fine tuning of the protonated/neutral species ratio.[21a–d]

If the stimulation by a chemical input such as pH changes can be advantageously used in chemical sensor field; its replacement by a photo or an electrochemical stimulation is highly desirable as they are considered as a more convenient manner to reach a spatial addressability in molecular electronic. As consequence, this study is devoted to the design of vinylpyrimidine chromophores **1**–**3** bearing a triphenylamine unit that can be electrochemically stimulated to reach the same protonated state than after acidic stimulation (Figure 1).

Results and Discussion

Synthesis

Compounds **1**–**3** were obtained by Knoevenagel condensation of 4-methylpyrimidine with the corresponding formyl derivatives of triphenylamine in boiling 5 M aqueous sodium hydroxide solution in the presence of Aliquat 336 as phase transfer catalyst according to the conditions developed for the synthesis of styrylpyrimidine derivatives (Schemes S1–S2).[22]

Acidochromic properties

As expected all three compounds exhibit similar UV-visible spectra in acetonitrile (ACN) with a band around 400 nm and a less intense band at higher energy. The enhancement of the electron donor character by the introduction of both methyl groups induces a slight bathochromic effect (~7 nm) between compound **1** and **2** on both bands. The addition of a second vinylpyrimidine substituent on the triphenylamine core in the structure of compound **3** leads to a large hyperchromic effect on the whole spectrum by a factor 1.65 (Figure 2). We can notice also a slight structuration of the low energy band with a maximum absorption wavelength at 413 nm and a shoulder around 380 nm.

To rationalize this behavior, theoretical studies based on the density functional theory (DFT) and by its time dependent extension (TD-DFT) have been performed. In such purpose 3 common exchange-correlation functionals have been used with IEFPCM solvation model. As expected, classical B3LYP appears as the less reliable one. If the global trend of absorption maximum wavelength variation between all three derivatives is well reproduced, the values are very largely redshifted. In fact, a difference ranging from 50 to 80 nm is observed between simulated vertical excitation wavelengths by TD/B3LYP/6-311G + (d) and experimental values (see SI). At the opposite, functions with long-range corrections such as M06-2X, CAM-B3LYP appear more appropriate to study molecular systems with evident charge transfer feature. Both functionals provide very reliable results where the maximum absorption wavelengths are slightly underestimated but CAM-B3LYP function provides highest blue shifted values (see SI). Nevertheless, the overall trends between all three derivatives are well reproduced as presented on Figure 2 for M06-2X function. As we can see, the 7 nm bathochromic shift between compound **1** and **2** experimentally observed is almost perfectly reproduced by quantum calculations (+6 nm).

This behavior can be explained by the enhancement of the electron donor character of the triphenylamine resulting from the insertion of the two methyl groups. Indeed, their insertion leads to an increase of the energy values of HOMO and HOMO-1 by ~0.1 eV whereas the LUMO level is almost unaffected (+0.03 eV) by this structural modification (Figure 3). More importantly, it is possible to assign from TD-DFT calculations the main absorption band to a π-π* transition with an internal charge transfer (ICT) character involving a transition from the HOMO to the LUMO orbitals respectively (Table 1). In this context, we can presume that the bathochromic shift experimentally noticed results from an enhancement of the charge transfer. To confirm this difference in CT process between compound **1** and **2**, the electron density difference in the transition process have been computed according to the

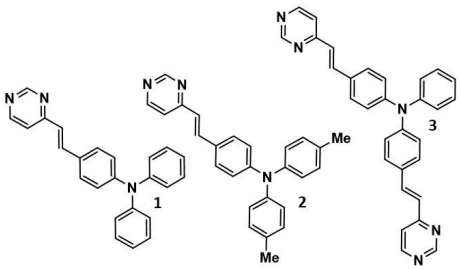

Figure 1. Structure of the vinylpyrimidime substituted triphenylamines **1**–**3**.

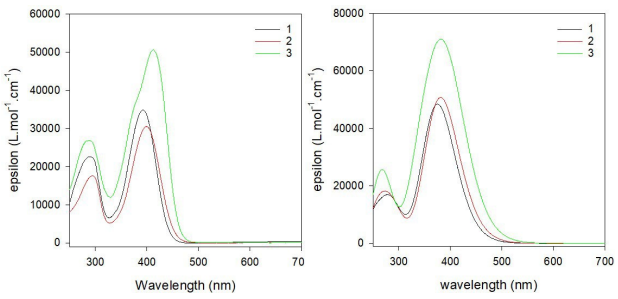

Figure 2. (left) Experimental and (right) simulated using TD/M06-2X/6-311G + (d,p) UV-Visible spectra in ACN of the three different triarylamine derivatives solution.

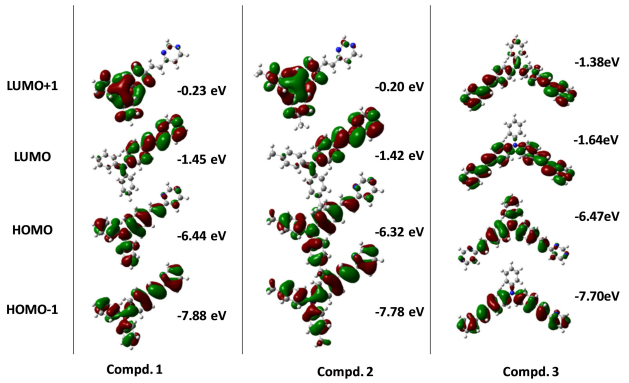

Figure 3. Shape and energy levels of the molecular orbitals from HOMO-1 to LUMO + 1 for the three triphenylamine derivatives **1**–**3** as computed at the M06-2X/6-311G(d,p) level in acetonitrile (IEF-PCM).

Table 1. Main electronic transitions for the three triphenylamine derivatives **1**–**3**.[a]

Compd.	λ_{exp}	ΔE_{ge}	λ_{ge}	f_{ge}	contribution
1	392	3.31	375	1.194	H→L (89%)
	290	4.32	288	0.248	H→L + 3 (90%)/
		4.53	274	0.105	H−1→L (50%)
					H→L + 4(21%)
2	399	3.25	381	1.253	H→L (88%)
	296	4.32	287	0.251	H−1→L + 3 (88%)
3	413	3.15	394	1.423	H→L (99%)
		3.57	348	0.778	H→L + 1 (99%)
	288	4.56	272	0.299	H−1→L (99%)
		4.71	264	0.193	H−1→L + 1 (53%)
					H→L + 2 (40%)

[a] Vertical excitation wavelengths (λ_{ge}, nm), vertical excitation energies (ΔE_{ge}, eV) and oscillator strengths (f_{ge}) calculated at TD/M06-2X/6-311G + (d,p)/IEF-PCM(acetonitrile) level of theory.

procedure described by Pr. D. Jacquemin and coworkers.[23] No strong variation between both compounds was observed on their electron density difference plots (see SI) which confirms a displacement of the electronic density from the triphenylamine to the vinylpyrimidine substituent. As expected, slight lower values for the amount (0.68 *vs* 0.69 e) and distance (4.3 *vs* 4.4 Å) of charge transfer are obtained for **1** in comparison to derivative **2**.

Concerning compound **3**, as observed for compounds **1** and **2**, TD-DFT calculations carried out by the help of functions involving long-range corrections (M06-2X and CAM-B3LYP) provide similar and more reliable results in comparison to B3LYP which largely overestimate the absorption maximum wavelength (see SI). As presented in Figure 2, spectrum computed at M06-2X/6-311G + (d,p)/IEF-PCM(ACN) level reproduces the hyperchromic effect on the main absorption band as well as its enlargement. These results can be explained by first the slight improvement of the oscillator strength (+20%) but more certainly by a new electronic transition at close energy involving the LUMO + 1 level. Indeed, this later is strongly stabilized (−1.38 eV) by the insertion of a second pyrimidine unit in comparison to compounds **1** and **2** (−0.23 and −0.20 eV respectively).

As expected, the addition of some acid (aq. HCl) to the solution induces an important modification of their absorption spectrum in all cases. As example for compound **2**, the addition leads to the appearance of a new band at 503 nm with the concomitant decrease of the band at 399 nm (Figure 4). A hypo and a bathochromic effect on the band at higher energy is also noticed with the appearance of a low intensity band at 333 nm. The presence of three isosbestic points at 311, 339 and 438 nm suggests an equilibrium between two species which is assigned to the selective protonation of the pyrimidine unit.[24] Nevertheless, a large excess of acid is requested to fully displace this equilibrium to the protonated form in agreement with the reported poor to medium Hydrogen-bond basicity of pyrimidine.[25]

Indeed, once protonated, the system should behave as a classical push-pull dye where the generated pyrimidinium unit acts as a strong withdrawing electron group. To confirm this hypothesis, DFT and TD-DFT quantum calculations on the different forms of compound **2** resulting from the protonation of the pyrimidine unit or the central nitrogen have been performed. The protonation of the central nitrogen atom leads to an increase of HOMO-LUMO gap by more than 1 eV depending on the level of theory used (B3LYP, M06-2X or CAM-B3LYP).

Such kind of protonation should then be discarded as it should conduct logically to observe an hypsochromic shift of the maximum absorption wavelength below 400 nm with the acid aliquots addition in disagreement with our experimental observations. At the opposite, the protonation of the pyrimidine (**2**+**H**$^+$) conducts to a decrease of the HOMO-LUMO gap and then a bathochromic effect. As expected for such push-pull dye, B3LYP function conducts to largely overestimate the maximum absorption wavelength of **2**+**H**$^+$ (λ_{max} = 549 nm). At the opposite, functions involving long-range corrections (M06-2X and CAM-B3LYP) predict more suitable similar results (with λ_{max} = 471 and 453 nm respectively) leading to observe for the first excited state a reduction of the vertical excitation energies of 0.62 and 0.59 eV respectively with the protonation of the pyrimidine unit, in agreement with the 0.64 eV experimentally noticed. Finally, the competition between the protonation of the triphenylamine core and the pyrimidine unit(s) can be

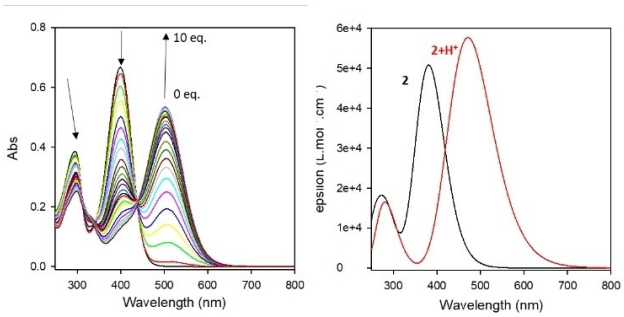

Figure 4. UV-Visible spectra changes of a solution of **2** in ACN (0.02 mM) upon addition of HCl aliquots (left) and simulated UV/vis absorption spectra of **2** and **2**+**H**$^+$ calculated at the TD/M06-2X/6-311 + (d,p)/IEF-PCM(acetonitrile) level of theory (right).

completely discarded by computation of the Gibbs free energy for corresponding reaction when TFA is used as acid. Computed at M06-2X/6-311G+(d,p)/IEF-PCM(ACN) level of theory, the protonation of the central nitrogen atom is much larger thermodynamically unfavorable than the pyrimidine unit with ΔG° values at 298 K of 98.4 are 39.3 kJ/mol respectively. Noticeably, the back conversion from $\mathbf{2+H^+}$ to **2** without noticeable degradation can be reached by using a base. In fact, addition of NEt_3 allow to restore the initial spectrum of the solution allowing to confirm the acid/base switching behavior (see Figure S6).

With two vinylpyrimidine substituents (compound **3**), two successive or simultaneous protonations of pyrimidine units leading to the formation of $\mathbf{3+H^+}$ and $\mathbf{3+2H^+}$ respectively have to be envisioned. If TD-DFT calculations suggest that both cations exhibit a different optical signature (Figure 5), a regular modification of absorption spectrum is noticed upon the addition of HCl (up to 7 eq.).

It is characterized by the appearance of a new band at 501 nm and the concomitant decrease of the band at 413 nm with the presence of isosbestic points suggesting only two species in equilibrium (Figure 5). The addition of a large excess of acid (conc. HCl) induces a modification of the spectrum translating by the complete disappearance of the band at 413 nm and the bathochromic shift of the lowest and highest energy bands at 515 and 321 nm respectively. Based on TD-DFT calculations, we can then presume that the second protonation of compound **3** is much less favorable than the first one and occurs only when a large excess of acid is introduced. Indeed, simulated spectra of $\mathbf{3+H^+}$ and $\mathbf{3+2H^+}$ present noticeable differences (Figure 5). If the first protonation leading to $\mathbf{3+H^+}$ induces the appearance of new strong absorption band at lower energy, it does not lead to a complete disappearance of the band in near UV region but to a large hypochromic effect revealing three distinct absorption bands. At the opposite, protonation of both pyrimidine units leading to $\mathbf{3+2H^+}$ is characterized by only two absorption bands largely red shifted in comparison to **3** as experimentally noticed when only a large excess of acid is added.

This successive protonation of pyrimidine units hypothesis is comforted by computed ΔG°(298 K) at M06-2X/6-311G+(d,p)/IEF-PCM(ACN) level of theory when TFA is used as acid. With a value of 44.2 and 44.0 kJ/mol for the first and second protonation respectively, both processes appear thermodynamically unfavorable. This explains also the requirement to larger acid amounts in order to displace the equilibrium in comparison to compound **2** protonation (ΔG°(298 K) = 39.3 kJ/mol).

In term of emission, as generally observed for diphenylamino substituted pyrimidines,[20a] the protonation of **1** and **2** leads to an emission quenching whatever the excitation wavelength (see SI for **2**).[16b] On the other hand the protonated form of **3** remained emissive in DCM as previously reported.[22c]

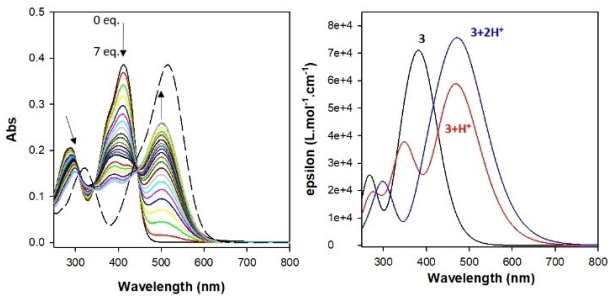

Figure 5. (Left) UV-Visible spectra changes of a solution of 3 in ACN (0.008 mM) upon addition of HCl (0 to 7 eq.) aliquots (solid line) and after adding an excess of HCl (dotted line). (Right) Simulated UV-Visible spectra of compound **3** in its neutral, monoprotonated ($\mathbf{3+H^+}$) and diprotonated ($\mathbf{3+2H^+}$) forms at the TD/M06-2X/6-311+(d,p)/IEF-PCM(acetonitrile) level of theory.

Electrochromic properties

Due to their numerous applications in molecular electronic field, the electrochemical behavior of triphenylamine derivatives has been largely investigated in the literature.[16,26] In this context, the electrochemical behavior of compounds **1**–**3** has been investigated by cyclic voltammetry and the resulting voltammograms are presented in Figure 6. If classical triphenylamine derivatives exhibit one reversible oxidation wave in a 0.3–0.5 V range (*vs* Fc/Fc^+) depending on the nature of the

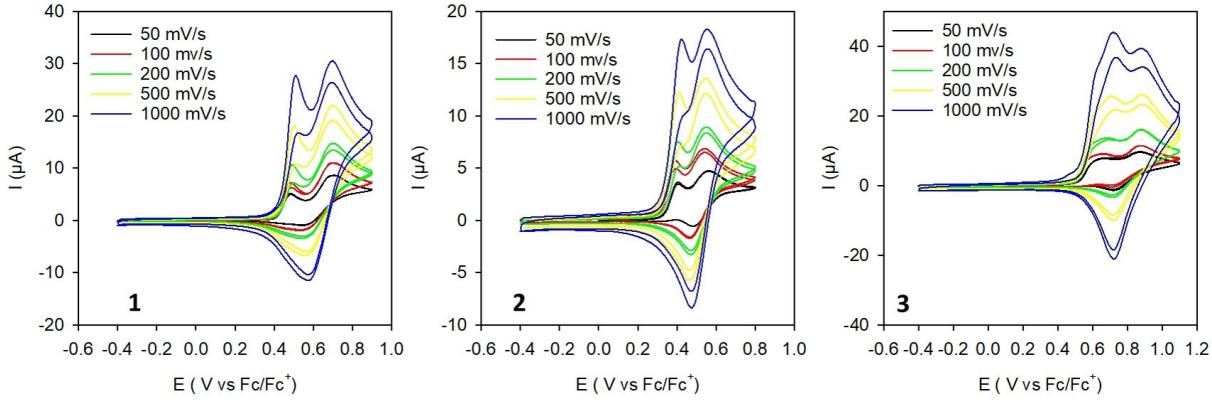

Figure 6. Cyclic voltammograms of derivatives **1**, **2** and **3** (1 mM) in 0.1 M $TBAPF_6$ /ACN solution at different scan rates.

substituent in *para* positions,[16,26] compounds **1**–**3** exhibit two successive anodic processes. The first one at 0.49, 0.39 and 0.63 V for compound **1**, **2** and **3** respectively is not reversible whatever the scan rate used. Based on previous study on triarylamine, this first process could be roughly explained by a two steps irreversible electrochemical mechanism: (*i*) the oxidation of the triphenylamino core leads to the corresponding radical cation, usually stable in our experimental conditions, in agreement with the HOMO localization (Figure 3), (*ii*) followed by an irreversible chemical process suggested by the irreversibility of the signal noticed for derivatives **1**–**3** even at 1000 mV.s^{-1}. To explain this second step, an oxidative dimerization process is generally suggested.[17] Results obtained discard this hypothesis because compound **2** presents two methyl groups on the *para* position as blocking substituents and exhibits similar behavior. In place, we presume a delocalization of the radical on the pyrimidine unit which is able to abstract an Hydrogen atom to surrounding media and form the corresponding protonated form. In this context, the second anodic process ranging from 0.52 to 0.80 V could be assigned to the oxidation of triphenylamino core of the corresponding protonated form as summarized on scheme 1 for compound **2**.

Such behavior would explain the difference of reversibility observed on the second oxidation process. In fact, only compound **2** exhibits a reversible oxidation wave whatever the scan rate used. At the opposite, compounds **1** and **3** exhibit an irreversible signal at low scan rate and its almost full reversibility is only restored for scan rate beyond 500 mV.s^{-1} (figure 6). Indeed, the first oxidation process should lead to their protonated **1**+**H**$^+$ and diprotonated **3**+**2H**$^+$ forms respectively which present some unsubstituted para positions. The generation of corresponding radical dication species during the second process could be then lead to oxidative dimerization process as neither blocking group presence nor a possible delocalization of the radical are present to avoid it.

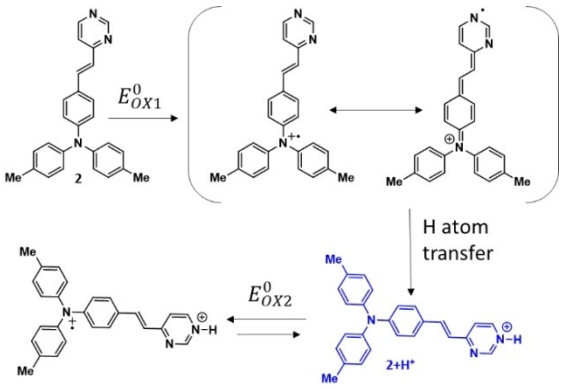

Scheme 1. Proposed route to explain the formation of the protonated form of compound **2** under an electrochemical stimulation.

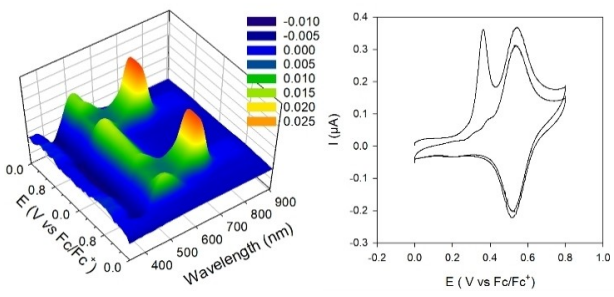

Figure 7. Spectroelectrochemistry (Left) in TLCV (right) conditions (~50 μm; 10 mV.s^{-1}) of **2** (1 mM) in ACN with (TBA)PF_6 (0.1 M) as an electrolyte on a platinum electrode.

In order to confirm the spontaneous evolution of the radical cation species generated during the first oxidation process to its corresponding protonated forms, spectro-electrochemical measurements have been performed with Thin Layer Cyclic Voltammetry (TLCV) technique. As an example, Figure 7 depicts the variation of the absorption spectrum of a solution of compound **2** as a function of the applied potential. As we can see, when the potential reaches 0.3 V an intense coloration of the solution is observed due to the appearance of a new band in the 500–550 nm range, and the decrease of the absorbance around 400 nm.

More importantly, the modifications of the UV-Visible absorption spectra during the first oxidation process are fully consistent with ones noticed during the titration of compound **2** by acid (figure 3) and then support the hypothesis of the generation of **2**+**H**$^+$ under an electrochemical stimulation. This efficient formation of **2**+**H**$^+$ under an electrochemical stimulation have been easily confirmed by treating a solution of **2** by an oxidizing reagent and monitoring the reaction by UV-Visible spectroscopy. Indeed, the uses of $NOSbF_6$ (0.87 V *vs* Fc/Fc^+)[27] was largely reported for such purpose to evidence mixed valence in electroactive species[28] or generating one-electron oxidation of organic donors.[29] As noticed with acid, the addition of $NOSbF_6$ aliquots to a solution of compound **2** leads to observe a bathochromic shift of the low energy band and an hypo and a bathochromic effect on the band at higher energy assigned to **2**+**H**$^+$ (see SI). As expected, the complete transformation of the system is observed after one equivalent of oxidizing agent. Concerning the back conversion of the system to its initial state, two different stimulations can be used indifferently. Indeed, the initial spectrum can be restored by adding either some hydrazine hydrate, a well-known reducing agent[30] (−0.178 V *vs.* reversible hydrogen electrode)[31] or some triethylamine as a base (see Figures S6&S8).

As a consequence, the substitution of a triphenylamine core by a vinylpyrimidine substituent leads to a bi-modal molecular switch as the interconversion between neutral and protonated form can be induced by using indifferently acid or an electrochemical stimulation.

Applying a redox potential higher than 0.5 V leads to a new modification of the absorption spectrum. As shown on Figure 7 for compound **2**, we notice a strong bathochromic and hyperchromic shift of the band at lower energy from 529 to 691 nm and a new band at higher energy around 380 nm. Based on previous studies about triphenylamine derivatives,[32] such behavior seems to translate the formation of the radical dication species (**2**+**H**)$^{2+\bullet}$, which is stable enough in these

experimental conditions due to the presence of the two methyl groups. The absorption spectrum corresponding to the protonated form $\mathbf{2+H^+}$ is regenerated on the back scan as soon as the applied potential decrease below 0.5 V. During the second cycle, any new variation is observed below 0.5 V as well as no residual peak of the first oxidation process (Figure 6). This hypothesis is supported by TD-DFT calculations. Indeed, computed absorption spectra of $(\mathbf{2+H})^{2+\bullet}$ at M06-2X/6-311G + (d,p)/IEF-PCM(ACN) level of theory reveals several electronic transitions at close energy leading to observe one broad absorption band with a λ_{max} value of 611 nm (Figure 8). As consequence, the first oxidation process should theoretically lead to observe a decrease of the absorbance at 373 nm with a concomitant increase of the absorbance at 479 nm due to the spontaneous evolution of the radical cation and the generation of $\mathbf{2+H^+}$. By applying a higher electrochemical potential, the generation of the dicationic radical species $(\mathbf{2+H})^{2+\bullet}$ should then induces a strong bathochromic effect (-0.56 eV) as experimentally noticed (-0.55 eV).

In addition, the oxidation potentials of each form have been evaluated by the help of DFT calculations for all three compounds. Indeed, theoretical redox potentials relative to the normal hydrogen electrode (NHE) could be deduced from calculated Gibbs free energy change according to the following expression (Eq (1)):

$$E^0 vs\ NHE = \frac{\Delta G^0_{solv}}{F} - 4.44 \quad (1)$$

Where F is the Faraday constant and 4.44 the free energy change (in eV) associated with the reference NHE half-reaction.[33] Following the methodology reported by Guo and Liu,[34] the variation of the Gibbs free energy change, ΔG^0_{solv}, induced by the oxidation reaction have been determined using B3LYP/6-311G(d) as basis set and IEF-PCM as solvation model. To overcome the underestimation of the adiabatic ionization potential by this method, 0.28 eV is generally added to the B3LYP results,[34] allowing to predict theoretical redox potentials in acetonitrile with a 0.17 V standard deviation for a large variety of organic compounds.[34] Computed redox potentials reproduce well the general trend experimentally observed but they are systematically underestimated by at least 0.1 V for compounds **1**–**3** (referenced as E^0_{ox1}) when the potentials of their corresponding monoprotonated forms ($\mathbf{1\text{-}2+H^+}$), E^0_{ox2}, and diprotonated forms ($\mathbf{3+2H^+}$), E^0_{ox3}, are more close to the experimental values. If the choice of B3LYP function to calculate ΔG^0_{solv}concerning molecular systems with evident charge transfer feature could be raised, it is important to remind that anodic peak potentials, generally reported for irreversible oxidation process, strongly depend on the scan rates, the sample concentration, and the kinetics of interfacial electron transfer especially when side reactions deplete the analyte from the electrode surface.[35] Moreover, the combination of 4.44 V as corresponding to standard potential of NHE in aqueous solution and SCE potentials (0.64 V) in order to reproduce the redox potential of the Fc^+/Fc couple in a nonaqueous solution can lead to drastic discrepancies.[36] In this context, we have changed the B3LYP function by M06-2X or CAM-B3LYP involving long-range corrections to calculate ΔG^0_{solv} and use directly 4.980 V as absolute reduction potential of the Fc^+/Fc couple in acetonitrile[36] for reference. As consequence, a new set of theoretical oxidation potential are obtained following Equation (2) and gathered in Table 2.

$$E^0\ vs\ Fc^+/Fc = \frac{\Delta G^0_{solv}}{F} - 4.980 \quad (2)$$

As we can see, the global trends experimentally observed as nicely reproduced whatever the exchange-correlation functional used. As example, an 0.1 V cathodic shift between compound **1** and **2** is well predicted and consistent with the enhancement of the electron donor character of the triphenylamine with the insertion of two methyl groups. Nevertheless, the best prediction for the different first oxidation potential is provided by M06-2X when calculated oxidation potential for their fully protonated forms present higher values than experimentally noticed. Surprisingly, this anodic shifts appears more important for $\mathbf{3+2H^+}$ and $\mathbf{1+H^+}$ (+0.14 and +0.08 V

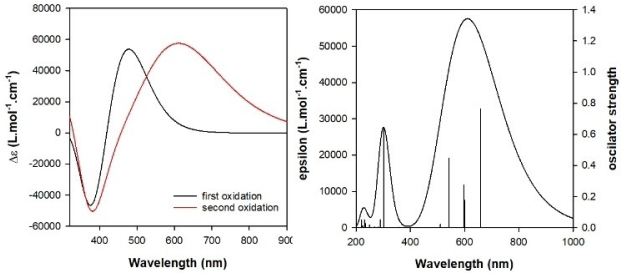

Figure 8. (right) Computed UV/vis absorption spectra of $(\mathbf{2+H})^{2+\bullet}$ at the TD/M06-2X/6-311 + (d,p)/IEF-PCM(acetonitrile) level of theory and (left) corresponding variation of the absorption properties of a solution of **2** by its first and second oxidation process.

Table 2. Experimental oxidation potentials (V *vs* Fc/Fc^+) of derivatives **1**–**3** in ACN and computed values under their neutral (E^0_{ox1}), monoprotonated (E^0_{ox2}) and diprotonated form (E^0_{ox3}).

Compd.[b]	Experimental		B3LYP[a]			M06-2X[b]			CAM-B3LYP[c]		
	E^{pa}_{ox1}	E^0_{ox2}	E^0_{ox1}	E^0_{ox2}	E^0_{ox3}	E^0_{ox1}	E^0_{ox2}	E^0_{ox3}	E^0_{ox1}	E^0_{ox2}	E^0_{ox3}
1	0.49	0.64	0.39	0.68	n/a	0.51	0.72	n/a	0.42	0.61	n/a
2	0.39	0.52	0.29	0.54	n/a	0.38	0.57	n/a	0.32	0.51	n/a
3	0.63	0.80	0.37	0.63	0.87	0.58	0.75	0.94	0.39	0.60	0.79

[a] Calculated at B3LYP/6-311G + (d)/IEF-PCM(ACN) level of theory. [b] Calculated at M06-2X/6-311G + (d,p)/IEF-PCM(ACN) level of theory [c] Calculated at CAM-B3LYP/6-311G + (d,p)/IEF-PCM(ACN) level of theory.

respectively) than for $2+H^+$ (+0.05 V) where any dimerization oxidation process could occur.

More importantly, computed oxidation potentials suggest the possibility to induce the selective formation of $3+H^+$ and $3+2H^+$ under an electrochemical stimulation with corresponding computed oxidation potential at 0.58 and 0.75 V respectively. However, the presence of a second vinylpyrimidine unit did not affect at a first glance the electrochemical behavior. As we can see on figure 6, compound **3** exhibits almost a similar voltammogram to compound **1**–**2** with two successive oxidation processes. However, one can notice a broadness of the first oxidation wave with a highest anodic peak potential (0.63 V) compared to compounds **1** and **2**. Increasing the scan rate leads to a splitting of this oxidation wave which let us presume the coexistence of different oxidation processes at close potentials. This assumption is confirmed by TLCV measurement where a clear splitting of the first oxidation process is noticed (Figure 9).

As we can see on figure 9, the voltabsorptograms confirm the transformation of compound **3** to its protonated forms $3+H^+$ and $3+2H^+$. Unfortunately, their close absorption maximum wavelength (*vide supra*) did not allow us to detect their successive formation along the variation of applied potential. Indeed, the absorbance around 410 nm starts to decrease as soon as the potential reaches 0.35 V and a concomitant increase in the 500–550 nm region. However, the maximum of this variation is gradually red shifted from 513 to 533 nm when applied potential ranges from 0.35 to 0.70 V (Figure 9).

Based on our observation during the titration of **3** by acid aliquots, such bathochromic effect can only suggest that the first oxidation process lead to the successive generation of the $3+H^+$ and $3+2H^+$ but with a poor selectivity. Applying a higher electrochemical potential conducts to observe a strong modification of the voltabsorptograms which show an intense absorbance at 703 nm and the emergence of a new signal at 356 nm during the second oxidation process. As in the case of compound **2**, this behavior can be assigned to the oxidation of $3+2H^+$ leading to corresponding radical cation. This hypothesis is fully supported by computed absorption spectra of $(3+2H)^{3+\bullet}$ at M06-2X/6-311G+(d,p)/IEF-PCM(ACN) level of theory (see SI). Indeed, the coexistence of the $3+H^+$ and $3+2H^+$ and their intrinsic proportion during the first oxidation process did not induce a strong variation of the voltabsorptograms where the intensities and the position of the minimum and maximum are slightly affected (Figure 10). At the opposite, the generation a radical from the oxidation of $3+2H^+$ during the second oxidation process should induce an enhancement of the absorbance especially in near UV region associated with an important redshift of the absorption in the visible range in agreement with experimental observations (Figure 10).

To confirm the successive generation of the $3+H^+$ and $3+2H^+$ under an electrochemical stimulation suggested by TLCV and spectroelectrochemical measurements, the titration of compound **3** by an oxidizing agent ($NOSbF_6$) have been performed. As shown on Figure 11, an irregular evolution of the UV-Visible spectra is observed when the quantity of oxidant increase. Up to 1 eq. the appearance of a new band at 504 nm is noticed as well as the concomitant decrease of the band at 413 nm. An hypo and a bathochromic effect on the higher energy band is also detected. More importantly, the presence of three isosbestic points at 306, 348 and 442 nm is observed translating an equilibrium between two species. Based on our results with acid, we can then assume that up to one equivalent, the addition of this oxidizing agent leads predominantly to the monoprotonated form ($3+H^+$). The further additions of $NOSbF_6$ induce a batho and hyperchromic effect of the main absorption band from 504 to 516 nm. With the decrease of the absorbance around 400 nm and the appearance of a new transition centered at 324 nm, these absorption spectrum changes are identical to those induced by the

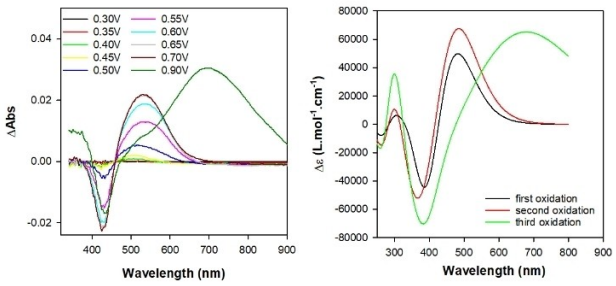

Figure 10. (left) Variation of the absorption spectra of a solution of **3** as function of the applied potential and (right) computed spectra variation at TD/M06-2X/6-311G+(d,p)/IEF-PCM(ACN) level of theory.

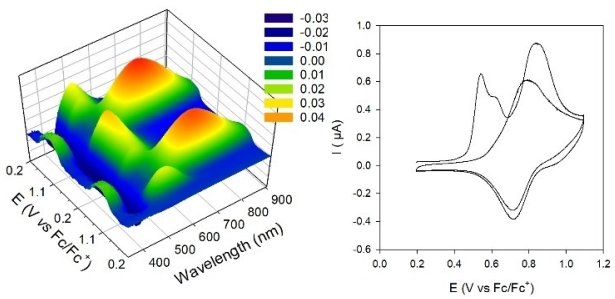

Figure 9. Spectroelectrochemistry (left) in TLCV (right) conditions (~50 μm; 10 $mV.s^{-1}$) of **3** (1 mM) in ACN with $(TBA)PF_6$ (0.1 M) as an electrolyte on a platinum electrode.

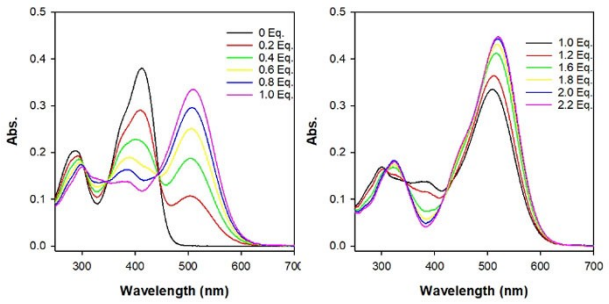

Figure 11. UV-Visible spectra changes of a solution of **3** in ACN (0.008 mM) upon addition of $NOSbF_6$ from 0 to 1.0 eq. (left) and from 1.0 to 2.2 eq (right).

addition of a large excess of acid and, as consequence, can be assigned to the generation of the diprotonated form ($\mathbf{3+2H^+}$). More importantly, this increment of the oxidizing agent quantity did not allow maintaining the observation of the three previous isosbestic points (306, 348 and 442 nm) which are replaced by two ones at 346 and 421 nm translated a new equilibrium between $\mathbf{3+H^+}$ and $\mathbf{3+2H^+}$ forms.

We can then conclude that an electrochemical stimulation of compound **3** leads to the successive formation of $\mathbf{3+H^+}$, $\mathbf{3+2H^+}$ and its corresponding radical $\mathbf{(3+2H)^{3+\bullet}}$ at higher potential allowing to switch its absorption maximum wavelength from near-UV to visible and finally almost near-IR region.

Conclusion

In summary, we have successfully developed a series of bimodal switches based on vinylpyrimidine-functionalized triphenylamines. These compounds can reach the same metastable state electrochemically, by applying a redox potential or a chemical oxidation, as by acidic stimulation. To explain these interesting bimodal switching abilities, the delocalization of the triphenylamine radical cation has been suggested. Mainly localized on the central triphenylamine core, this later is able to be delocalized to the peripheral vinylpyrimidine unit which, after abstraction of a hydrogen atom from the surrounding media, leads to the formation of the corresponding protonated form. Generally requiring an excess of acid due to the moderate hydrogen-bond basicity of the pyrimidine ring, the protonated forms of the different systems can then be generated in a more efficient and controlled way by an electrochemical stimulation. This later opens the way to induce a step by step addressability of molecular systems as well as a modulation of the molecular property over several discrete levels. As demonstrated with compound **3**, bearing two vinylpyrimidine fragments, the chemical oxidation permits to reach successively the monoprotonated $\mathbf{3+H^+}$ and diprotonated $\mathbf{3+2H^+}$ forms. If the first protonation induces a strong modification of the maximum absorption wavelength, the second protonation of the system leads only to a moderate, red-shifted absorption. In addition to their potential applications as colorimetric indicators, the structural variation along their stimulation from nonpolar to dipolar and finally quadripolar dyes is promising for these systems as acido/redox NLO switches and are currently under investigation.

Experimental Section

General information regarding synthesis and spectroscopic characterization can be found elsewhere.[21c] Compounds **1** and **3** were obtained according to reported procedure.[22b–c]

Synthesis of (*E*)-4-(4-di(*p*-tolyl)aminoystyryl)pyrimidine (**2**): A stirred mixture of 4-methylpyrimidine (141 mg, 1.5 mmol) and 4-(di-p-tolylamino)benzaldehyde (451 mg, 1.5 mmol) in aqueous sodium hydroxide (5 M, 15 mL) containing Aliquat 336 (64 mg, 0.15 mmol) was heated under reflux for 2 h. The mixture allowed to cool, and the precipitate was filtered off, washed with water and purified by silica gel column chromatography using AcOEt as eluent. Yellow solid, yield 53% (301 mg) *Rf* (AcOEt) = 0.42; mp = 130-132 °C (AcOEt); ^{1}H NMR (300 MHz, $CDCl_3$) δ 9.13 (s, 1H), 8.62 (d, ^3J = 5.1 Hz, 1H), 7.83 (d, ^3J = 15.9 Hz, 1H), 7.43 (d, ^3J = 8.4 Hz, 2H), 8.62 (d, ^3J = 5.1 Hz, 1H), 7.12 (d, ^3J = 7.8 Hz, 2H), 7.06-7.6.98 (m, 6H), 6.90 (d, ^3J = 15.9 Hz, 1H), 2.35 (s, 6H); ^{13}C NMR (75 MHz, $CDCl_3$) δ 162.8, 158.8, 157.0, 149.6, 144.5, 137.3, 133.6, 130.1, 128.7, 127.9, 125.4, 122.5, 120.9, 118.2, 20.9. HRMS (ESI+, TOF) *m/z* calculated for $C_{26}H_{23}N_3$ (M^+) 377.1886; found 377.1886.

Quantum chemical calculations: Full geometry optimizations of compound **1**–**3** as well as their diverse protonated form were performed based on density functional theory (DFT) using three different exchange-correlation functional (B3LYP, CAM-B3LYP and M06-2X) with the 6-311G(d) or 6-311G(d,p) basis sets. All optimized structures correspond to stationary points on the potential energy surfaces, as confirmed by only real vibrational frequencies. Linear optical properties were determined at the time-dependent DFT level using corresponding functionals with a basis set including diffuse function. Solvent (acetonitrile) effects were included in all calculations by means of the polarizable continuum model in its integral equation formalism (IEF-PCM).[37]

UV-Vis titration: UV-Vis spectra were registered on a Shimadzu UV-1800 spectrometer from solutions in ACN (HPLC grade) from VWR chemicals. In agreement with our previous studies, titrations were performed using either freshly prepared daily $NOSbF_6$ (Sigma-Aldrich) solution in ACN or a HCl solution in ACN prepared by successive dilution from brand new aqueous solution of HCl (37% from VWR chemicals).

Cyclic voltammetry: ACN (HPLC grade) and tetra-*N*-butylammonium hexafluorophosphate (TBAP, electrochemical grade, Fluka was recrystallized from ethanol). Cyclic voltammetry (CV) was performed in a three-electrode cell equipped with a platinum millielectrode, a platinum wire counter-electrode and a silver wire used as a quasi-reference electrode. The electrochemical experiments were carried out under a dry and oxygen-free atmosphere ($H_2O < 1$ ppm, $O_2 < 1$ ppm) in ACN with TBAP (0.1 M) as the support electrolyte. The voltammograms were recorded on a potentiostat/galvanostat (BioLogic – SP150) driven by the EC-Lab software with positive feedback compensation. All the potential reported were calibrated versus Ferrocene/Ferrocenium oxidation potential (+ 0.405 V *vs* SCE or + 0.425 V *vs* Ag/AgCl).

Time-resolved spectroelectrochemistry was performed using the already described home self-made cell described elsewhere.[38] A distance of 25–200 μm between the surface of the electrode and the optical window was typically used in our experiments. Electrochemical measurements were carried out using a platinum wire counter electrode and a silver wire as a quasi-reference electrode with a Biologic SP-150 potentiostat driven by the EC-Lab software including ohmic drop compensation. Experiments were recorded in dry HPLC-grade ACN with TBAP (electrochemical grade, Fluka) as supporting electrolyte. All solutions were prepared and transferred into the spectroelectrochemical cell in a glove box containing dry, oxygen-free (< 1 ppm) argon, at room temperature. Spectrophotometric measurements were carried out with a homemade bench composed of different PRINCETON INSTRUMENTS modules (light sources, fibers, monochromators, spectroscopy camera and software). To start the two experiments at the same time, the two benches are synchronized with TTL signals.

Acknowledgements

The authors gratefully acknowledge the CARMA platform (SFR MATRIX, Univ. Angers) for their assistance in spectroscopic analyses. They also acknowledge IC3EM organizers for providing suitable environment for the emergence of fruitful collaborations.

Conflict of Interest

The authors declare no conflict of interest.

Data Availability Statement

The data that support the findings of this study are available from the corresponding author upon reasonable request.

Keywords: acidity · electrochemistry · molecular switches · triphenylamine · pyrimidine

[1] B. L. Feringa, *Molecular Switches*, Wiley-VCH Verlag GmbH **2001**, pp. i–xxii.
[2] a) L. Zhang, H. X. Wang, S. Li, M. H. Liu, *Chem. Soc. Rev.* **2020**, *49*, 9095–9120; b) B. L. Feringa, *J. Org. Chem.* **2007**, *72*, 6635–6652; c) J.-X. Wang, C. Li, H. Tian, *Coord. Chem. Rev.* **2021**, *427*, 213579.
[3] a) A. Fihey, A. Perrier, W. R. Browne, D. Jacquemin, *Chem. Soc. Rev.* **2015**, *44*, 3719–3759; b) M. M. Lerch, M. J. Hansen, W. A. Velema, W. Szymanski, B. L. Feringa, *Nat. Commun.* **2016**, *7*, 12054; c) M. Jeong, J. Park, S. Kwon, *Eur. J. Org. Chem.* **2020**, *2020*, 7254–7283.
[4] a) L. Liu, P. Liu, L. Ga, J. Ai, *ACS Omega* **2021**, *6*, 30189–30204; b) S. Erbas-Cakmak, S. Kolemen, A. C. Sedgwick, T. Gunnlaugsson, T. D. James, J. Yoon, E. U. Akkaya, *Chem. Soc. Rev.* **2018**, *47*, 2228–2248.
[5] a) Y. Feng, M. Ovalle, J. S. W. Seale, C. K. Lee, D. J. Kim, R. D. Astumian, J. F. Stoddart, *J. Am. Chem. Soc.* **2021**, *143*, 5569–5591; b) C. Cheng, J. F. Stoddart, *ChemPhysChem* **2016**, *17*, 1780–1793.
[6] a) A. Abdollahi, H. Roghani-Mamaqani, B. Razavi, *Prog. Polym. Sci.* **2019**, *98*, 101149; b) G. Pasparakis, M. Vamvakaki, *Polym. Chem.* **2011**, *2*, 1234–1248.
[7] Q. Tang, X. Meng, H. Jiang, T. Zhou, C. Gong, X. Fu, S. Shi, *J. Mater. Chem.* **2010**, *20*, 9133–9139.
[8] a) H. Ren, P. Yang, F. M. Winnik, *Polym. Chem.* **2020**, *11*, 5955–5961; b) W. Zhao, D. Zou, Z. Sun, Y. Xu, G. Ji, X. Li, C. Yang, *Adv. Theor. Simul.* **2020**, *3*, 2000163.
[9] L. Kortekaas, W. R. Browne, *Chem. Soc. Rev.* **2019**, *48*, 3406–3424.
[10] a) V. A. Barachevsky, V. G. Butenko, *Russ. J. Gen. Chem.* **2018**, *88*, 2747–2772; b) W. R. Browne, B. L. Feringa, *Chimia* **2010**, *64*, 398–403.
[11] Y.-D. Cai, T.-Y. Chen, X. Q. Chen, X. Bao, *Org. Lett.* **2019**, *21*, 7445–7449.
[12] G. Szalóki, L. Sanguinet, *Photon-Working Switches* (Eds.: Y. Yokoyama, K. Nakatani), Springer Japan, Tokyo **2017**, pp. 69–91.
[13] a) S. Zhuang, X. Li, J. Liu, *Dyes Pigm.* **2021**, *193*, 109464; b) L. Zhang, W. Zhan, Y. Dong, T. Yang, C. Zhang, M. Ouyang, W. Li, *ACS Appl. Mater. Interfaces* **2021**, *13*, 20810–20820; c) H.-J. Yen, G.-S. Liou, *Polym. Chem.* **2012**, *3*, 255–264; d) H.-J. Yen, G.-S. Liou, *Polym. Chem.* **2018**, *9*, 3001–3018; e) H.-J. Yen, G.-S. Liou, *Org. Electron.* **2010**, *11*, 299–310.
[14] J. Wang, K. Liu, L. Ma, X. Zhan, *Chem. Rev.* **2016**, *116*, 14675–14725.
[15] C. Cabanetos, P. Blanchard, J. Roncali, *Chem. Rec.* **2019**, *19*, 1123–1130.
[16] S. Dapperheld, E. Steckhan, K. H. G. Brinkhaus, T. Esch, *Chem. Ber.* **1991**, *124*, 2557–2567.
[17] a) E. T. Seo, R. F. Nelson, J. M. Fritsch, L. S. Marcoux, D. W. Leedy, R. N. Adams, *J. Am. Chem. Soc.* **1966**, *88*, 3498–3503; b) M. Thelakkat, *Macromol. Mater. Eng.* **2002**, *287*, 442–461.
[18] a) Z. L. Gong, C. J. Yao, J. Y. Shao, H. J. Nie, J. H. Tang, Y. W. Zhong, *Sci. China Chem.* **2017**, *60*, 583–590; b) J. H. Tang, Y. Q. He, J. Y. Shao, Z. L. Gong, Y. W. Zhong, *Sci. Rep.* **2016**, *6*.
[19] a) D. B. Zhang, J. Y. Wang, D. Jacquemin, Z. N. Chen, *Inorg. Chem. Front.* **2016**, *3*, 1432–1443; b) A. Wolf, E. Moulin, J. J. Cid, A. Goujon, G. Y. Du, E. Busseron, G. Fuks, N. Giuseppone, *Chem. Commun.* **2015**, *51*, 4212–4215; c) R. Sakamoto, S. Kume, H. Nishihara, *Chem. Eur. J.* **2008**, *14*, 6978–6986.
[20] a) S. Achelle, J. Rodríguez-López, F. Bureš, F. Robin-le Guen, *Chem. Rec.* **2020**, *20*, 440–451; b) T. Sachdeva, S. Gupta, M. D. Milton, *Curr. Org. Chem.* **2020**, *24*, 1976–1998; c) E. Cariati, C. Dragonetti, E. Lucenti, F. Nisic, S. Righetto, D. Roberto, E. Tordinab, *Chem. Commun.* **2014**, *50*, 1608–1610.
[21] a) S. Achelle, J. Rodríguez-López, C. Katan, F. Robin-le Guen, *J. Phys. Chem. C* **2016**, *120*, 26986–26995; b) J. Tydlitát, S. Achelle, J. Rodríguez-López, O. Pytela, T. Mikýsek, N. Cabon, F. Robin-le Guen, D. Miklík, Z. Růžičková, F. Bureš, *Dyes Pigm.* **2017**, *146*, 467–478; c) Z. I. M. Allaoui, E. le Gall, A. Fihey, R. Plaza-Pedroche, C. Katan, F. Robin-le Guen, J. Rodríguez-López, S. Achelle, *Chem. Eur. J.* **2020**, *26*, 8153–8161; d) R. Plaza-Pedroche, D. Georgiou, M. Fakis, A. Fihey, C. Katan, F. Robin-le Guen, S. Achelle, J. Rodríguez-López, *Dyes Pigm.* **2021**, *185*; e) U. Giovanella, E. Cariati, E. Lucenti, M. Pasini, F. Galeotti, C. Botta, *ChemPhysChem* **2017**, *18*, 2157–2161; f) D. Liu, Z. Y. Zhang, H. Y. Zhang, Y. Wang, *Chem. Commun.* **2013**, *49*, 10001–10003.
[22] a) J. J. Vanden Eynde, L. Pascal, Y. Van Haverbeke, P. Dubois, *Synth. Commun.* **2001**, *31*, 3167–3173; b) S. Achelle, A. Barsella, C. Baudequin, B. Caro, F. Robin-le Guen, *J. Org. Chem.* **2012**, *77*, 4087–4096; c) A. I. Aranda, S. Achelle, F. Hammerer, F. Mahuteau-Betzer, M.-P. Teulade-Fichou, *Dyes Pigm.* **2012**, *95*, 400–407.
[23] a) I. Ciofini, T. Le Bahers, C. Adamo, F. Odobel, D. Jacquemin, *J. Phys. Chem. C* **2012**, *116*, 11946–11955; b) D. Jacquemin, T. Le Bahers, C. Adamo, I. Ciofini, *Phys. Chem. Chem. Phys.* **2012**, *14*, 5383–5388.
[24] F. Kournoutas, I. K. Kalis, M. Feckova, S. Achelle, M. Fakis, *J. Photochem. Photobiol. A.* **2020**, *391*, 112398.
[25] M. Berthelot, C. Laurence, M. Safar, F. Besseau, *J. Chem. Soc. Perkin Trans. 2* **1998**, 283–290.
[26] a) P. Agarwala, D. Kabra, *J. Mater. Chem. A.* **2017**, *5*, 1348–1373; b) X. Lian, Z. Zhao, D. Cheng, *Mol. Cryst. Liq. Cryst.* **2017**, *648*, 223–235.
[27] J. K. Kochi, *Acc. Chem. Res.* **1992**, *25*, 39–47.
[28] a) Y. Cotelle, M. Hardouin-Lerouge, S. Legoupy, O. Alévêque, E. Levillain, P. Hudhomme, *Beilstein J. Org. Chem.* **2015**, *11*, 1023–1036; b) Y. F. Ran, C. Blum, S. X. Liu, L. Sanguinet, E. Levillain, S. Decurtins, *Tetrahedron* **2011**, *67*, 1623–1627.
[29] T. Sasamori, N. Tokitoh, R. Streubel, *Organic Redox Systems* (Ed.: T. Nishinaga), John Wiley & Sons, **2016**.
[30] A. Furst, R. C. Berlo, S. Hooton, *Chem. Rev.* **1965**, *65*, 51–68.
[31] K. Asazawa, K. Yamada, H. Tanaka, M. Taniguchi, K. Oguro, *J. Power Sources* **2009**, *191*, 362–365.
[32] C. Quinton, V. Alain-Rizzo, C. Dumas-Verdes, F. Miomandre, G. Clavier, P. Audebert, *RSC Adv.* **2014**, *4*, 34332–34342.
[33] S. Trasatti, *Pure Appl. Chem.* **1986**, *58*, 955–966.
[34] Y. Fu, L. Liu, H.-Z. Yu, Y.-M. Wang, Q.-X. Guo, *J. Am. Chem. Soc.* **2005**, *127*, 7227–7234.
[35] E. M. Espinoza, J. A. Clark, J. Soliman, J. B. Derr, M. Morales, V. I. Vullev, *J. Electrochem. Soc.* **2019**, *166*, H3175–H3187.
[36] M. Namazian, C. Y. Lin, M. L. Coote, *J. Chem. Theory Comput.* **2010**, *6*, 2721–2725.
[37] J. Tomasi, R. Cammi, B. Mennucci, *Int. J. Quantum Chem.* **1999**, *75*, 783–803.
[38] O. Alévêque, E. Levillain, L. Sanguinet, *Electrochem. Commun.* **2015**, *51*, 108–112.

Manuscript received: July 20, 2022
Revised manuscript received: October 5, 2022
Accepted manuscript online: October 11, 2022
Version of record online: November 16, 2022